Synergistic Voltaglue adhesive mechanisms with alternating electric fields

*Manisha Singh[1,2], Cheong See Yin[2], Samuel J. Page[3], Yuqing Liu[4,5], Gautama Wicaksono[2], Rajashekhar Pujar[6], Shyam Kumar Choudhary[7], Giridhar U. Kulkarni[6], Jun Chen[4], John V. Hanna[2,3], Richard D. Webster[8], Terry W. J. Steele[1,2]**

[1]NTU-Northwestern Institute for Nanomedicine (NNIN), Interdisciplinary Graduate School (IGS), Nanyang Technological University (NTU), 50 Nanyang Drive, Singapore 637553

[2]School of Materials Science and Engineering (MSE), Nanyang Technological University (NTU), Singapore 639798

[3]Department of Physics, University of Warwick, Coventry CV4 7AL, United Kingdom

[4]ARC Centre of Excellence for Electromaterials Science, Intelligent Polymer Research Institute (IPRI), Australian Institute of Innovative Materials (AIIM), University of Wollongong, Wollongong, NSW 2522, Australia

[5]State Key Laboratory of Electronic Thin Film and Integrated Devices, University of Electronic Science and Technology of China, Chengdu, 610054, China.

[6]Centre for Nano and Soft Matter Sciences, Jalahalli, Bengaluru 560013, India

[7]Tata steel LTD, Jamshedpur 831001, India

[8]Division of Chemistry and Biological Chemistry, School of Physical and Mathematical Sciences, Nanyang Technological University, Singapore 637371

*Correspondence to Terry W. J. Steele (e-mail: wjsteele@ntu.edu.sg)

ABSTRACT

Voltage-activated adhesion is a relatively new discovery that relies on direct currents for initiation of crosslinking. Previous investigations have found that direct currents are linearly correlated to the migration rates of electrocuring, but this is limited by high voltages exceeding 100 V with instances of incomplete curing of voltage- activated adhesives on semiconducting substrates. Practical applications of electrocuring would benefit from lower voltages to mitigate high voltage risks, especially with regard to potential medical applications. Alternative electrocuring strategies based on alternating current (AC), electrolyte ionic radius, and temperature are evaluated herein. Square waveform AC electric fields are hypothesized to initiate a two-sided curing progression of voltage-activated adhesive (PAMAM-g-diazirine aka Voltaglue), where initiation occurs at the cathode terminal. Structure-activity relationships of AC frequency at currents of 1-3 mA are evaluated against direct currents, migration rate, storage modulus, and lap shear adhesion on *ex- vivo* tissue mimics. Numerous improvements in electrocuring are observed with AC stimulation versus DC, including a 35 % decrease in maximum voltage, 180 % improvement in kinetic rates, and 100 % increase in lap shear adhesion at 2 mA. Li^+ ion electrolytes and curing at 4 ^oC shift curing kinetics by +104 % and -22 % with respect to the control ion (Na^+ ion at 24 ^oC), suggesting electrolyte migration is the rate limiting step. Li^+ ion electrolytes and curing at 50 ^oC improves storage modulus by 110% and 470 % respectively. Further evaluations of electrocured matrices with ^{19}F NMR, solid-state NMR and infrared spectroscopy provide insights into the probable crosslinking mechanisms.

INTRODUCTION

Voltage-activated adhesives are a new platform of stimuli responsive materials[1-4]. Motivation behind their development is a result of limitations in adhesive initiation and controlling subsequent material properties. Some of these limitations are: (i) uncontrolled kinetics in two-part adhesives, (ii) short pot-lives of adhesives mixed in batches (iii) energy required for heating

and cooling the molds for thermoset resins, and (iv) requirement of initiators, preservatives, and transparent surfaces for photo-activated adhesives. In addition to addressing these limitations, an adhesive that is initiated/propagated by voltage would allow simple electronic interfacing—which is ideal for manufacturing efficiency.

Voltaglue is an example of voltage-activated adhesives, in which aryl-diazirine (electrochemical crosslinker) is grafted onto the surface of a polyamidoamine (PAMAM) dendrimer. PAMAM dendrimers are commercially available in a number of sizes and a choice of surface functionalization[5-17]. Aryl-diazirine is an ambient stable precursor that can be activated by heat (>100 ^{o}C), UVA, or voltage.

Voltaglue possesses the unique capability of covalent crosslinking in the presence of electric fields. Voltaglue, as a model system for electrocuring, lacks the adhesion strength (< 100 kPa) reminiscent of epoxy and acrylate resins (> 1 MPa) but offers design advantages that allow exploration of electrocuring concepts. Previous evaluations of Voltaglue using direct current (DC) stimulation have elucidated its tunable material properties, soft tissue adhesion, application in organic solvents, and its activation on semiconducting tapes[1-4, 18-19]. Despite evaluating DC stimulation on a number of electrode geometries, limitations such as—incomplete curing, weak mechanical properties, and requirement of high voltage electric fields >2 V/mm are still present. Voltaglue undergoes one-sided electrocuring progression from the cathode to the anode under DC activation. Cyclic voltammetry (CV) investigations display quasi-chemically reversible behavior that converts to complete chemical reversibility in aprotic mediums when the scan rate approaches 2 V/s [4]. In order to circumvent limitations related to DC stimulation, alternating currents (AC) are hypothesized to remedy incomplete curing because complete progression is sought by taking advantage of two-sided electrocuring migration from the cathode to the anode. As the direction of the applied current would change,

cathode (-) and anode (+) terminals would switch alternately, resulting in a two-sided electrocuring.

A square waveform AC is hypothesized to maintain the same efficacy as DC, where current amplitude would be maintained at the same level (1-3 mA) to allow efficiency comparisons. Structure-activity relationships of AC frequency and current amplitude are evaluated on the migration rate, shear modulus, gelation time, and adhesion strength. This work also explores the hypothesized carbene intermediate mechanism of electrocuring via Fourier transform infrared spectroscopy (FTIR), nuclear magnetic resonance (NMR), counter-cation, and temperature assessments.

EXPERIMENTAL SECTION

MATERIALS

Polyamidoamine (PAMAM) dendrimer, Generation 5, Mw=28.8 kDa was bought from Dendritech, Inc, USA. 3-[4-(bromomethyl) phenyl]-3-(trifluoromethyl)- diazirine (bromo-diazirine) was purchased from TCI, Japan. Teledeltos paper (PK-9025B) was obtained from PASCO scientific, CA. Collagen casings were procured from Nippi, Japan.

METHODS

Synthesis of PAMAM-g-diazirine (aka Voltaglue)

PAMAM-g-diazirine was synthesized in the same way as previously published[1-2, 4, 18, 20]. Herein, 20 % of the amine groups present on the surface of polyamidoamine (PAMAM) dendrimer were grafted by aryl- diazirine. The synthesized PAMAM-g-diazirine (20%) was dissolved in phosphate buffer saline (1X PBS) as 50 % w/w ratio to test structure-activity relationships and the resulting liquid formulation is referred to as Voltaglue throughout the text. All the experiments were conducted at 24 ^{o}C, unless stated otherwise.

Electrodes for AC stimulation

Teledeltos resistive electrodes were prepared as previously published[1]. A thin 1 cm^2 layer of liquid uncured Voltaglue (~ 30 mg) was spread equidistant from both copper tapes using a laboratory micro spatula.

The composite assembly of uncured Voltaglue and Teledeltos paper electrode is referred to as Voltaglue patch throughout the text (refer Figure S2 for illustration).

Alternating electric current source for AC stimulation

Electrocuring of Voltaglue on Teledeltos paper electrodes was energized via square waveform AC (1, 2, or 3 mA), applied with a 2450 Keithley's Source Meter Unit. The anode and cathode terminals of the Source Meter unit were connected to the two copper sides of the Voltaglue patch using alligator clips. Once electrical contacts were ensured, alternating current was applied, and the corresponding voltages were recorded. The AC frequencies investigated were 8-12500 mHz. The electrocuring progression of Voltaglue was tracked by digital photography at 30 FPS and evaluated with the software ImageJ. The recorded transparent (uncured) vs. opaque (electrocured) regions over the surface of the Voltaglue patch were quantified using the software ImageJ and the area of the opaque region is called as progression and is reported in mm^2.

Real-time electro-rheology of Voltaglue

Real-time viscoelastic parameters were evaluated with a parallel plate rheometer (Physica MCR 102, Anton Paar, 1% strain, 1 Hz oscillation, 0.2 mm gap size) setup. Voltaglue patch was supported with a custom jig, secured to the bottom plate to a Peltier heater (Peltier Universal Optical Device, P-PTD120 SN80670834), as previously reported[1]. Electric alternating currents of 1-3 mA were applied using a 2450 Keithley's Source Meter Unit. Electrical isolation was

maintained with a high impedance ceramic probe (disposable plate D-PP10/MX/S07) under ambient conditions.

Electrical impedance spectroscopy of the Voltaglue patch

Impedance measurements were performed with a two-electrode configuration using an Autolab Potentiostat (Metrohm Autolab, Netherlands) with a built-in frequency response analyzer. A voltage of 10 mV (rms) was used and the complex impedance was measured using a sinusoidal input voltage over a range of frequencies from 10^5 Hz to 0.1 Hz. The experimental data were fitted using Nova 2.1.

Lap shear adhesion assessment against wet collagen substrates

Collagen substrate sections (2 × 2 sq. cm) and Voltaglue patch (i.e. uncured bioadhesive spread over Teledeltos paper) were mounted on microscope slides with double-sided tape. Voltaglue patches were stimulated with 1, 2, or 3 mA AC for 10 min. Lap shear adhesion failure values were recorded at maximum force before failure with a 50 N load cell (Chatillon Force Measurement Products, USA), with a linear elongation of 3 mm min^{-1}.

^{19}F NMR spectroscopy analysis of cured Voltaglue

All cured, or uncured Voltaglue formulations were analyzed with NMR (Bruker Advance) at 400 MHz with DMSO-d6. Topspin software was used in peak assignment and peak integration of ^{19}F NMR spectra. Both uncured and electrocured samples were dissolved in DMSO-d6 at 10 mg mL^{-1}. After recording the NMR spectra of uncured and electrocured samples, a UVA light dose (365 nm) of 12 J cm^{-2} was irradiated on the NMR tubes containing the samples. The same NMR tubes were then used to record the UV-cured NMR spectra.

All solid state ^{19}F MAS NMR measurements were obtained using a 700 MHz Bruker Advance III HD spectrometer operating a ^{19}F Larmor frequency of 658.7 MHz. All measurements were facilitated utilizing a Bruker 1.3 mm HXY MAS probe operating at MAS frequency of 60 KHz.

The ^{19}F MAS NMR data were acquired through single pulse (Bloch decay) measurements which used a ^{19}F π/2 pulse time of 3 μs and a recycles delay of 5 s between the acquisition of each transient, with all data being externally referenced to a secondary solid reference of PTFE (δ_{iso} = -123.2 ppm).

^{19}F NMR: Voltaglue uncured (400 MHz; DMSO-d6) δ -64.6, -76.7. Voltaglue electrocured (400 MHz; DMSO-d6) δ -64.6, -76.7, -80.3. Voltaglue electro and UV cured (400 MHz; DMSO-d6) δ -56.4, -64.6, -76.7, -80.3. Voltaglue UV cured (400 MHz; DMSO-d6) δ -56.4, -64.6, -76.7, -80.3. Voltaglue electrocured solid state NMR (16.4 T, 60 kHz) δ -64.6, -76.7, -80.3.

FTIR analysis of cured Voltaglue

FTIR (PerkinElmer Frontier) measurements were performed with a Universal ATR fixture of a ZnSe crystal. Voltaglue patches were electrocured directly onto the crystal and each measurement was an accumulation of 64 scans with a resolution of 4 cm^{-1} and a scan range of 4000 to 600 cm^{-1}.

Colorimetric analysis using universal pH indicator

A universal pH indicator solution (in isopropanol, ACROS Organics) was mixed with 1X PBS (control) and Voltaglue. A weighing boat (5 cm long, 3 cm wide, and 0.5 cm deep) filled with 1X PBS to three-quarters of the boat was topped with 0.5 mL of pH indicator solution and two copper electrodes were suspended in the weighing boat at the opposite ends across its length. A 30 V DC was applied across copper terminals using a 2450 Keithley Source Meter Unit. Voltaglue was mixed with Universal pH Indicator Solution as 10% w/w and connected via Teledeltos paper to 3 mA DC or 3mA AC (50 mHz) using a Keithley 2450 Source Meter Unit.

Voltaglue electrocuring as a function of temperature and counter-cation

The effects of temperature and counter-cations (available in solvent 1X PBS) on electrocuring progression were investigated either by varying the temperature of the Voltaglue patch from 24 ^{o}C to 4 or 50 ^{o}C or by replacing the Na^{+}, available in 1X PBS, by a relatively heavier or lighter ion (i.e. K^{+}, or Li^{+}). The counter-cation used for all the temperature-based experiments was Na^{+} and the temperature used for all the counter-cation based experiments was 24 ^{o}C. The recipe of the saline solvents is provided in the supplementary information (Figure S9).

Statistical analysis

All data are presented as mean ± SD (n=3, unless stated otherwise). The significance was evaluated with OriginPro 2016 64-bit software by one-way ANOVA with Tukey correction as post-hoc test. $p < 0.05$ (*) were considered to be statistically significant. Rheology and lap shear adhesion was smoothed to remove transient noise by a Loess method with a span of 0.1.

RESULTS

Scope of electrocuring structure-activity relationships

Previous investigations of Voltaglue have observed incomplete curing (< 100% progression) and soft shear moduli of < 1 kPa under DC (1-3 mA) stimulation, despite multiple electrode configurations[1]. Direct currents up to 10 mA push the current sourcemeter to the 200 V limit with no significant improvements in mechanical and adhesion properties (see **Figure S1**). With a static electric field, initial migration rates were ~ 1-3 mm. min^{-1} at DC 1-3 mA, but decay rapidly. AC electric fields were predicted to have bidirectional electrocuring with an improvement in migration rates and attain 100 % progression. Herein, alternating currents of 1, 2, and 3 mA at varying frequencies on the Voltaglue patch assembly (**Figure S2**, **Table S1**) were interfaced to Voltaglue on semiconducting Teledeltos paper with the aid of a programmable sourcemeter. The sourcemeter provides dynamic voltage feedback to maintain the set current.

Previous cyclic voltammetry investigations displayed complete 1 e^- chemical reversibility in aprotic mediums (ACN solvent) at frequencies >1000 mHz, but no limit was reached in protic mediums (acetonitrile + acetic acid)[4]. A frequency range (8-12500 mHz) was chosen that covers the CV conditions and bridges the transition from DC to AC stimulation. An AC square waveform was chosen, as it offers the most direct comparison to DC migration rates. Other waveforms will be investigated in future work.

Voltaglue electrocuring progression was tracked visually through the evolution of nitrogen. The nitrogen evolution starts at the cathode and migrates to the anode, as seen in **Figure 1**. Under AC electric fields, the progression migrates from both directions as the bipolar electrodes are swapped. Digital images of progression with respect to frequency and time are available in **Figure S3**. Progression over a 10-min interval under 3 mA (f=50 mHz) is shown in **Figure 1B**. Crosslinking of Voltaglue patches was subsequently evaluated via real-time electrorheology to yield the storage/loss modulus, gelation time, and yield stress. Adhesion strength of the AC stimulated patches was tested against wet collagen substrates that serve as a soft tissue mimic. Additional analysis with ^{19}F NMR, FTIR, counter-cation, temperature, and semiconductor substrate provided further data towards elucidating the curing structure-activity relationships.

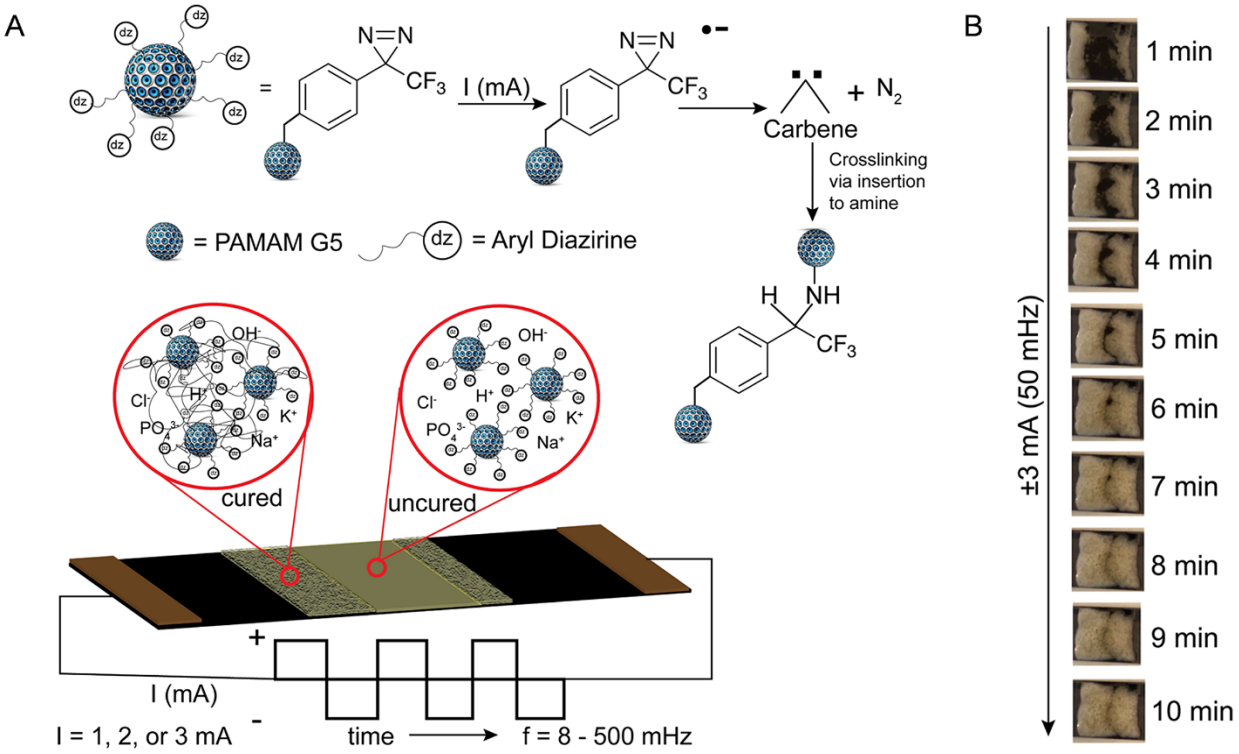

Figure 1: Overview of two-sided electrocuring progression of Voltaglue on the surface of Teledeltos paper. A) Hypothesized reaction mechanisms and illustration of two-sided progression of AC-mediated electrocuring on the Voltaglue patch. B) Representative digital images of two-sided electrocuring progression over a 10-min interval. Images were analyzed for surface area progression and migration rates. AC parameters: 3 mA square wave at 50 mHz or 20 s cycle times.

Improved progression under AC electrocuring at lower voltages than DC

Electrochemical impedance spectroscopy (EIS) estimates the frequency window of Voltaglue electrochemical reduction. Interpretation of the relative changes in the real and imaginary impedance components, the complex impedance is presented as Nyquist plots, where the reactance Z" versus the Z' resistance plotted as a function of frequency from 0.1 to 10^5 Hz in **Figure 2A**. Empirical data correlates to a 4-component electrical circuit model (**Figure S4,**

Table S2). Impedance spectroscopy suggests no charge interfaces exist above 25 Hz. Representative voltage data at 2 mA displays the dynamic voltage waveforms (**Figure 2B**), DC vs. AC peak voltages (**Figure 2C**), and maximum voltages required as a function of current at different frequencies (**Figure 2D**).

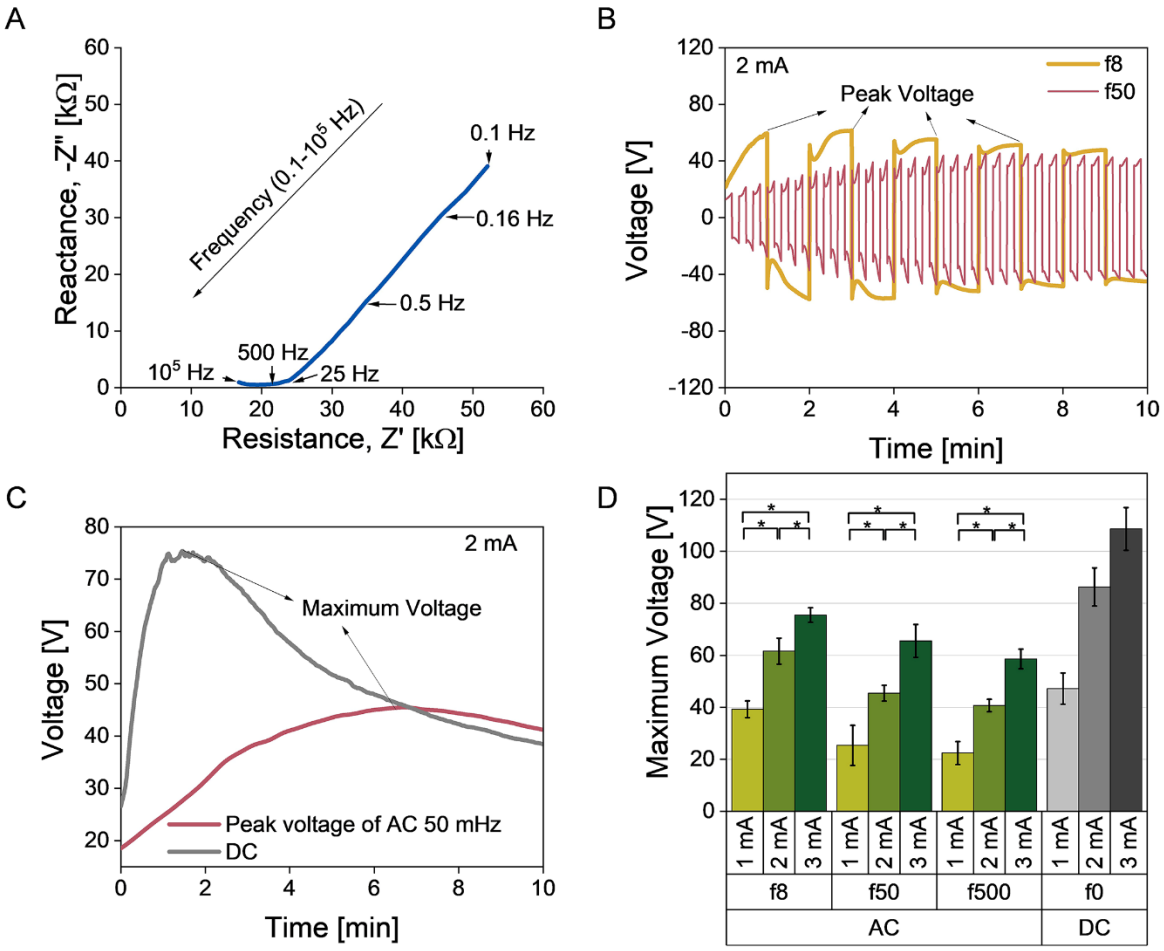

Figure 2: Electrochemical parameters of AC-mediated electrocuring. A) Electrochemical impedance spectroscopy of uncured Voltaglue at 0.1 to 10^5 Hz. B) Dynamic voltage waveforms at 2 mA AC as recorded during 10 minutes of electrocuring. C) 2 mA DC vs. AC peak voltages as function of time. D) Maximum voltages recorded during AC-mediated electrocuring as function of current and frequency.

Alternating current progresses electrocuring bidirectionally from the cathode to the anode. The progression of electrocured Voltaglue from the cathode to anode was evaluated by the change in transparent (uncured Voltaglue) to opaque (cured) surface, as seen in **Video S1**. AC stimulation at 500 mHz to 1000 mHz rapidly reduces the electrocuring progression, with negligible progression beyond 1000 mHz (**Figure S3**). A frequency of 8-500 mHz is the optimized range for analysis of structure-activity relationships for comparison to DC. Currents were limited to 1-3 mA. The contour plot in **Figure 3A** (inset) displays how progression rapidly decayed when the cycle time falls below 2 s (> 500 mHz).

Progression rates were determined by fitting the progression plots with a first order decay as shown in **Figure 3B** . The rate constants are summarized in **Table S3**. The maximum progression reached in case of 2 mA AC was 14 % higher than DC as seen in **Figure 3C**. **Figure 3D** compares the progression as a function of current and frequency. Progression increased with current but decayed with frequency. Complete progression can be seen with frequencies less than 1000 mHz, given enough time.

Teledeltos paper (5 kΩ/sq.) is an inexpensive model system to investigate the electrocuring under electrical stimulation but can be potentially replaced with other semiconductive substrates such as PEDOT:PSS or graphene oxide. A brief assessment of electrocuring progression was performed on gold (500 Ω/sq.), PEDOT:PSS (6 kΩ/sq.), and reduced graphene oxide (60 kΩ/sq.) coated substrates. The recorded progression is summarized in **Figure S5**. No electrocuring was observed over gold coated substrates and incomplete progression was observed on the relatively high resistance reduced graphene oxide. AC electrocuring on graphene interdigitated electrodes demonstrates AC is applicable to more discreet electrode designs (**Video S2**). DC activation was found to electrocure only on cathode electrode surfaces (50-60 % of the total electrode surface area). In contrast, AC was found to electrocure substantially higher surface areas (> 90%) than DC.

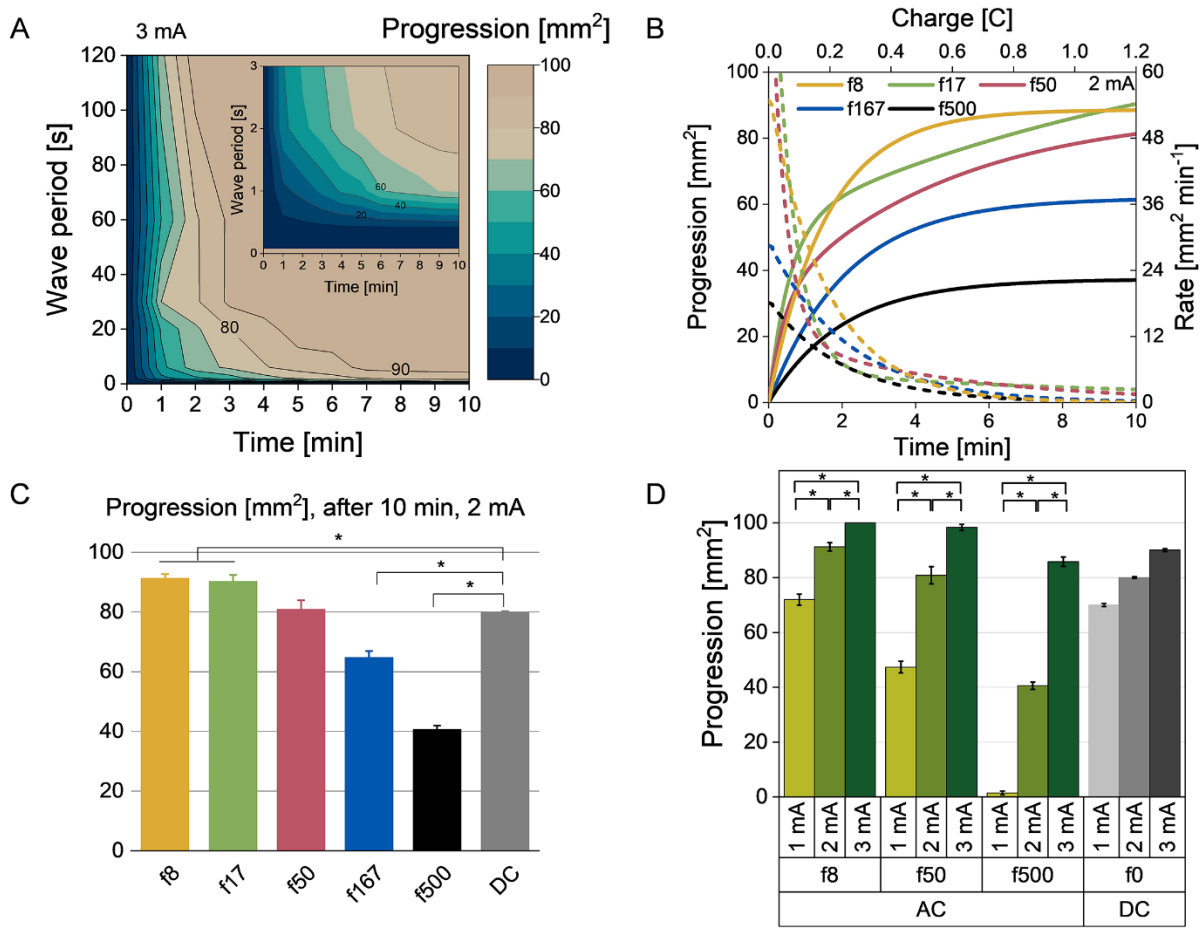

Figure 3: Dependence of electrocuring progression on AC magnitude and frequency. A) Contour plot of progression as a function of wave period and electrocuring time. 120 s corresponds to 8 mHz and 20 s corresponds to 500 mHz. B) Temporal progression of electrocuring at 2 mA alternating current. C) Progression comparison of AC electrocuring at a range of frequencies. D) Comparison of maximum progression after 10 minutes. Data presented as mean ± SD, n = 3, p-values are calculated using one-way ANOVA with Tukey correction, *p < 0.05.

238

239 **Optimized AC electrocuring improves mechanical and adhesion properties compared to**
240 **DC.**

Real-time electrorheology measures the Voltaglue crosslinking, under the application of square wave AC of 1, 2, and 3 mA at frequencies of 8-500 mHz. After the application of AC, an increase in the storage modulus (G') values was immediate **(Figure 4A, 'on' region)**. The gelation time, where G' = G", at frequencies of 8-500 mHz is summarized in **Figure S6**. The highest storage modulus of 1380 Pa (at 1% strain) was achieved after the application of 2 mA AC at 50 mHz (**Figure 4B**). This is an increase of 47% compared to the application of 2 mA DC. **Figure 4C** summarizes the storage modulus of Voltaglue under AC stimulation of 1-3 mA at different frequencies and current. Storage modulus generally increases with current but decreases with frequency. Parameters set at 50 mHz and 2 mA appear to optimize these opposing dependencies.

The adhesion strength of the electrically activated Voltaglue patch against a soft tissue mimic (collagen films) is analyzed via lap shear adhesion. Representative stress vs. strain curves as a function of 2mA, AC frequencies are displayed in **Figure 4D**. The mechanical modulus is seen to be dependent on the amount of shear strain applied, which accounts for the low storage moduli reported under rheometry (**Figure S6**). The maximum adhesion strength at failure is plotted in **Figure 4E** for 2 mA AC at different frequencies. The maximum adhesion strength at failure for 2 mA 50 mHz AC was 60 % higher than using 2 mA DC. Adhesion strength of Voltaglue under AC displayed no correlations to frequency or current, as observed in **Figure 4F**. Overall, the maximum adhesion strength achieved for AC was 33% higher than DC. The maximum voltage needed to reach this adhesion for AC was 59% lower than DC (**Figure 4F**, **Figure 2D**), indicating that AC allows a more efficient electrocuring. Adhesion strength of Voltaglue was comparable to the commercial sealant Dermabond® and 900 % higher than DuraSeal® (**Figure S7**).

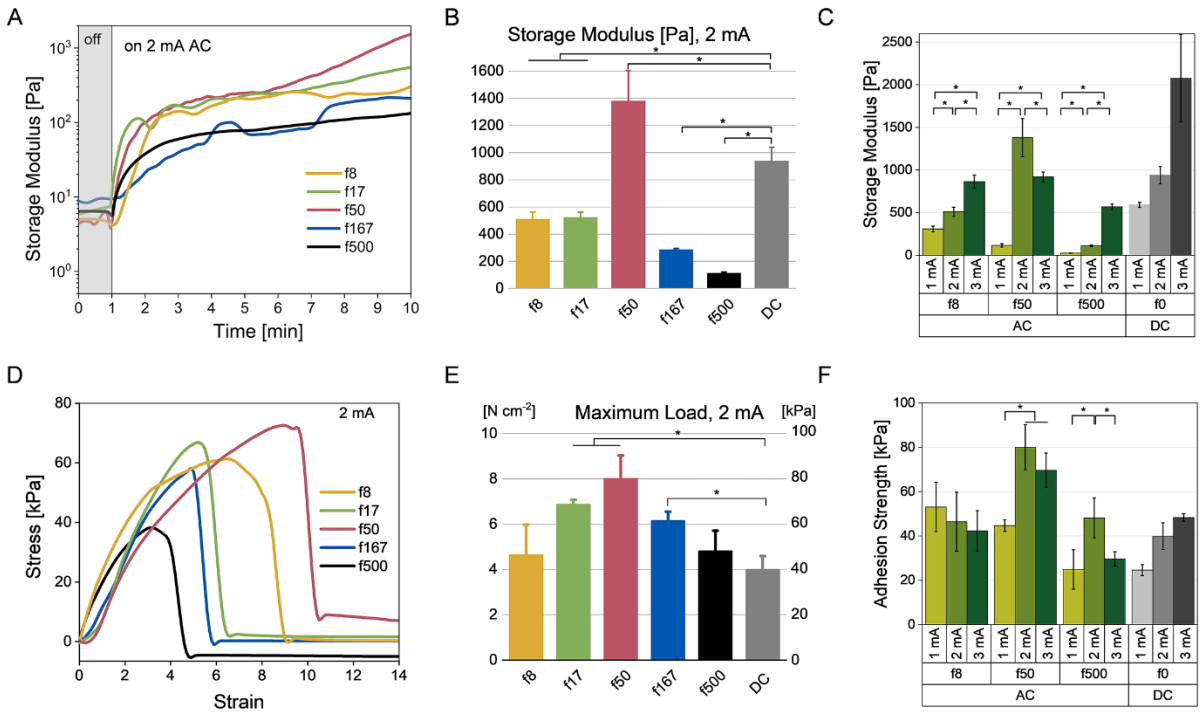

Figure 4: Frequency-mediated mechanical and adhesion properties of Voltaglue patch. A) Representative storage modulus (G') before and after 2 mA, AC stimulation at frequencies of 8-500 mHz. B) Maximum storage modulus after termination of alternating current of 2 mA at 10 min vs 2 mA, DC control. G' is determined at 1 % strain. C) Comparison of maximum storage modulus (G') at different AC levels (1- 3 mA) for different test frequencies. DC (1-3 mA) is used as a control. D) Representative stress vs. strain curves of lap shear adhesion at different AC (2 mA) frequencies. E) Maximum adhesive shear strength at failure after 10 min of electrocuring using AC (2 mA) at frequencies of 8-500 mHz. Control, DC-2 mA. F) Comparison of adhesive shear strength at failure at AC of 1-3 mA and frequencies. Control, DC (1-3 mA). Data presented as mean ± SD, n = 3, p-values are calculated using one-way ANOVA with Tukey correction, *p < 0.05.

264

265 **Spectroscopy confirms the consumption of diazirine with no diazoalkane intermediates**

The hypothesized mechanism of crosslinking and electrocuring progression is based on a transient diazirinyl radical that acts to propagate electrons and eventually form a metastable crosslinker. Therefore, insertion of nucleophilic functional group such as an amine on the surface of PAMAM is assumed to react with a metastable intermediate, e.g. diazoalkane, carbene. Both diazoalkane and carbene are known from photo activation of diazirine and carbene is known from thermal activation. One electron reduction of diazirine yields a stable and chemically reversible diazirinyl radical, which may lead to carbene formation. However, other cross-linking mechanisms cannot be excluded, including 1) diazirine isomerization to form diazoalkane (a known intermediate in photoactivation) with subsequent nucleophilic attack, 2) carbene attack on diazirine to form crosslinking azines, 3) amine oxidation at the anode, or 4) a combination of two or more mechanisms[21-26].

The $-CF_3$ group on the diazirine offers a sensitive method to illuminate new covalent bonds on the more stable singlet carbene. The solution and solid state ^{19}F NMR data for the uncured and electrocured samples are displayed in **Figure 5**. Electrocured samples appear to be insoluble in most organic solvents—extractions display only uncured Voltaglue. The corresponding ^{19}F NMR data (**Table 1)** indicates the consumption of the diazirine $-CF_3$, but no new resonances were detected in electrocured samples. Peak areas obtained for uncured, and electrocured samples were 3420, and 2234, respectively. This supports the reduction of diazirine and Voltaglue by 35 %, implying that diazirine is activated and consumed during electrocuring. No evidence of an azine resonance was seen in the ^{19}F NMR spectra, which is reported at δ_F ppm -66.8 to -66.9 [27]. Dissolved Voltaglue from uncured and electrocured samples were exposed to UVA light dose (365 nm) of 12 J/cm^2 where diazoalkane formation served as a positive control of diazirine photo-isomerization. Diazoalkane peaks in the photo-cured samples are displayed at δ_F ppm -56.4. No evidence of diazoalkane intermediates were observed in electrocured spectra — crosslinking does not occur through this metastable intermediate. Solid-state ^{19}F MAS NMR

evaluation of the electrocured powdered samples offers a more direct evaluation in **Figure 5B**, **Table 1.** If carbene insertion is present by primary amines or water, both will display insertion peaks at δ_F ppm -77 and -80. The ratio of diazirine (-64 ppm)/nucleophilic insertion (-77 ppm) dropped to 8/1 from an uncured initial value of 33/1.

Amine-based carbene insertion (vs. O insertion from water) is supported by comparative FTIR spectra in **Figure 6A**. Electrocuring decayed the primary amines at 3280 cm^{-1}. FTIR peak assignments are summarized in **Table 2**.

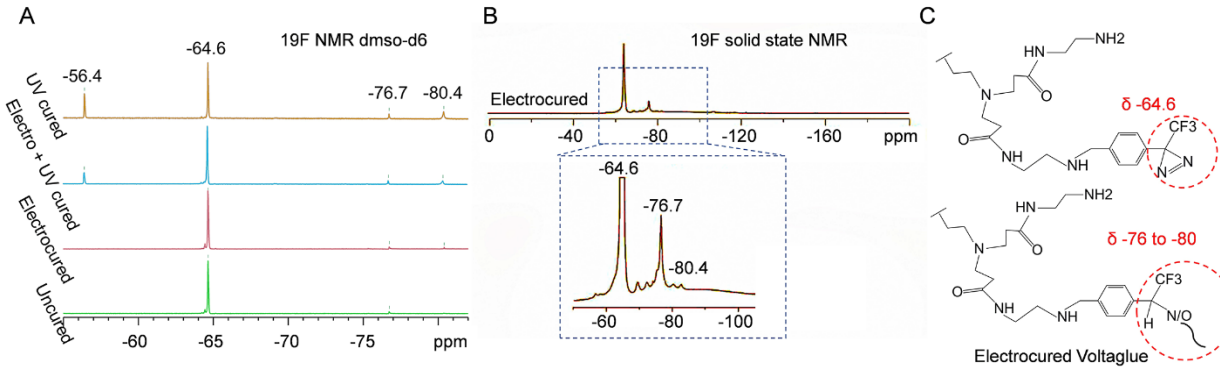

Figure 5: Comparative characterization of uncured and electrocured Voltaglue. A) ^{19}F solution NMR spectra of uncured, electrocured, both electro and UV-cured, UV cured Voltaglue samples; solvent: DMSO-d6 B) Solid state ^{19}F MAS NMR of electrocured powdered samples. C) Illustration of functional groups on Voltaglue corresponding to ^{19}F NMR data.

Table 1. 19F NMR integration of uncured, electrocured, and UV cured Voltaglue.				
Peak, δ_F ppm	**-56.4**	**-64.6**	**-76.7**	**-80.4**
Functional group	Diazoalkane	Diazirine	Insertion to amine or water	
Peak Integration				
Solution NMR (DMSO-d6)				

Uncured	0	3420	100	0
Electrocured	0	2234	100	59
Electro and UV cured	484	2195	100	185
UV cured	595	1204	100	273
Solid state NMR				
Electrocured	0	1250	156	10

299

300 Next, if it is hypothesized that if Voltaglue is generating nitrogen via carbene insertion, then
301 there should be no pH changes in the matrix. However, if the hydrogen or oxygen evolution
302 occurs through electrolysis, pH changes would be observed with colorimetric pH indicators as
303 shown in **Figure 6B** with aqueous PBS. To test this hypothesis, universal pH indicator was
304 mixed with Voltaglue/PBS as displayed in **Figure 6B**. Voltaglue, upon DC stimulation,
305 undergoes a drop in pH at the anode, but no color change at the cathode or progression front.
306 This supports the supposition of N_2 emission at the cathode (and not H_2). However, there is a
307 pH change at the anode ($[OH]_{aq}^- \longrightarrow ¼\ O_2 + ½\ H_2O + e^-$). The removal of OH^- led to a rapid
308 decrease in pH. Oxidation at the anode appears to be balancing the diazirine reduction to
309 diazirinyl. However, when Voltaglue mixed with the universal pH indicator was placed under an
310 AC of 3 mA (50 mHz), little to no color change was observed.

311 Temperature and counter-cation effects were investigated to improve complete progression and
312 kinetics as shown in **Figure 6C** and **6D**. The differential curves (dotted) are used to calculate
313 the rate constants (k) which were 0.37, 0.72, and 0.76 min^{-1} for 4, 24, and 50 ^oC, respectively.
314 The k-values corresponding to different cations were measured as 0.39, 0.72, and 0.75 min^{-1} for
315 K^+, Na^+, and Li^+, respectively. With regards to temperature, the most remarkable observation
316 was the 38 % drop in maximum voltage (**Figure S8)**. Shifts in G' are summarized in **Figure 6E**.

An increase of 470 % was observed in G' by increasing the temperature from 25 ºC to 50 ºC. The rheometry temperature sweep in **Figure S8C** demonstrates no thermal crosslinking, indicating the increase in G' at 50 ºC is due to electrocuring through a lower activation energy, faster ionic diffusion (lower viscosity), or both. An increase of 110 % was observed in G' by changing the counter-cation from Na^+ to Li^+, which is attributed to faster ionic diffusion.

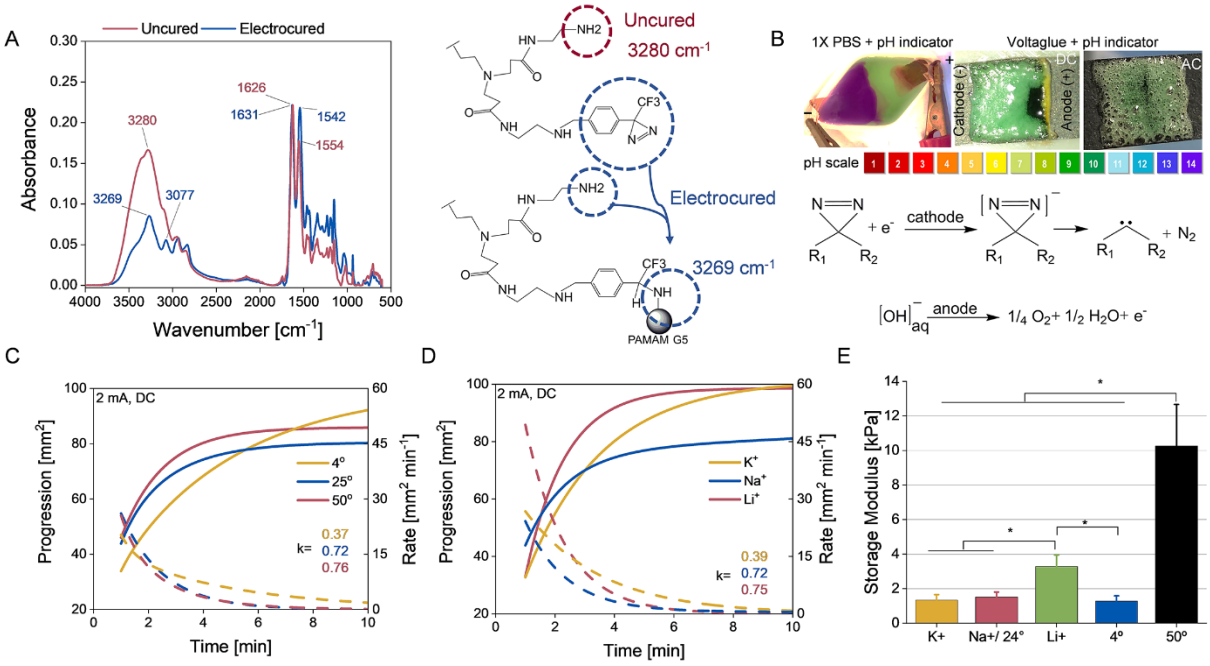

Figure 6: Characterization and optimization of electrocured Voltaglue. A) FTIR spectra of uncured and electrocured Voltaglue formulation, displaying a drop in –NH2 band (3280 cm^{-1}). Peaks were normalized to carbonyl band at 1631 cm^{-1}. B) Colorimetric pH indicator of aqueous PBS undergoing 30 V water electrolysis at both the cathode and anode (left); Voltaglue mixed with pH Indicator solution on Teledeltos paper with a 3 mA/100 V DC (middle); 3 mA AC at 50 mHz (right). A pH decrease occurs at the anode, no pH change is observed at the cathode. C) Progression and rate analysis as a function of temperature. D) Progression and rate analysis as a function of counter-cation. E) Storage modulus as a function of temperature and counter-cation after 10-min electrocuring at 2 mA DC.

Table 2. FTIR spectra of Voltaglue	
Functional group	**FTIR Peak (cm^{-1})**
–NH2–	3280
$–CH_2–$	2954 and 2833
C=N/C=O	1743
–CO-NH– I[a]	1626
–CO-NH– II[b]	1554
C-N	1344
C-F	1152
[a] –CO-NH– I i.e. Amide I is governed by stretching vibrations of C=O. [b] –CO-NH– II i.e. Amide II is governed by in-plane N-H bending.	

DISCUSSION

Voltage-curable adhesives (aka Voltaglue) have been evaluated under AC towards optimizing progression, kinetics, and material properties. Square waveform AC-stimulated curing of Voltaglue on the surface of Teledeltos paper (aka Voltaglue patch) migrates from the cathode to anode resulting in a two-sided progression as opposed to only one-sided progression in the case of DC[1]. AC-mediated crosslinking was followed by real-time evaluation of viscoelastic properties (**Figure 4**). The mechanical modulus was tuned within 0.5 Pa-10 kPa values, which lie within the range observed for most soft tissues (0.1 Pa-10 kPa)[28-30]. This has implications for

mimicking tissue compliance with synthetic biomaterials at the biomaterial interface. Adhesion to collagen ranges from 25-82 kPa, which is 1.2 times higher when compared to DC electric fields[1], and 16-fold higher than commercially available fibrin glue (5 kPa)[31-32]. Tunable adhesion and cohesive failure may be beneficial for wound healing electrical treatments where low-risk wound trauma is desired during a change of dressings.

The complete progression of electrocuring is achieved at much lower electric fields of ≤ 2 V/mm with respect to AC whereas DC requires ≥ 5 V/mm (**Figure S1**, 150-180 V/30 mm). However, the underpinning mechanism that governs the kinetics is under evaluation. Kinetic, pH, FTIR, and ssNMR based mechanistic evaluations provide new insight into diazirine-based electrocuring. The kinetics were followed for various AC/DC current and frequency, at different temperatures, with or without substituting the counter-cation.

The storage modulus and adhesion strength are seen to be dependent on the amplitude and frequency of the electric current applied. This behavior may be attributed to combination and competition of several factors— (i) conversion of diazirine to diazirinyl radical leads to crosslinking, (ii) consumption of diazirinyl radical (to carbene) however leads to a drop in electron carriers, hence increase in resistance during electrocuring, (iii) diazirinyl radical concentration is limited by negative charge repulsion, (iv) cation migration relieves charge repulsion, but ion migration drops exponentially due to increase in the viscosity as Voltaglue electrocures. AC frequency of 50 mHz at 2 mA appears to balance this cascade of events. A low frequency/DC stimulation results in ion migration as the rate limiting step that governs the conversion of diazirinyl radical formation. High frequency relieves the ion migration, but may ultimately lower diazirinyl radical formation or radical lifetime.

These investigations (i) support that ionic diffusion is the rate-limiting step of cathode to anode progression, (ii) suggest that nitrogen is the main gas component of evolution, (iii) identify a refined list of possible electrocuring intermediates, (iv) hypothesize carbene insertion as the

most likely crosslinking candidate, and (v) demonstrate enhanced progression rates using AC at lower voltages than DC.

Electrostatic voltage gradient and resistance mismatch are proposed to mediate the electrocuring progression of Voltaglue on the surface of Teledeltos paper. The role of cations (K^+, Na^+, Cl^-, OH^-) in generating the electrostatic voltage gradient is further reinforced by the temperature and counter-cation based structure-activity relationships. The temperature-dependent and counter-cation kinetics exhibit increases in the rate constants and shear modulus (at 50 ^oC and Li^+) implying that ionic diffusion is a rate-limiting step with respect to progression and crosslinking reactions. This could be attributed to the decrease in complex modulus of uncured Voltaglue at higher temperature or faster diffusion of smaller cations. Counter-cation-based kinetics are analyzed through the ionic radii order as $Li^+ < Na^+ < K^+$ (crystal ionic radii of 90, 116, and 152 pm, respectively)[33]. Hydration ionic radii are unknown in these high solute conditions that are far from the ideal in which they are typically measured (10-100 mM)[34-35].

Inspection of Voltaglue when mixed with a pH indicator reveals a color change at the anode. Oxidation of OH^- ions at the anode leads to the creation of an enriched protic zone at the progression end. This explains the incomplete curing under low DC (1-4 mA) stimulation—a drop in pH will likely allow a $2e^-/2H^+$ reduction of diazirine (N=N) to diaziridine (HN-NH), which is supported by the previously postulated cyclic voltammetry (CV) analysis[4]. However, the oxidation mechanism must be more complex as higher DC (6-10 mA) will drive complete progression. In contrast, lower AC-mediated crosslinking prevents or dilutes the OH^- oxidation allowing complete progression. The absence of crosslinking in reduced pH environments suggests the crosslinking intermediate derives from the diazirinyl radical.

The ^{19}F NMR data rules out the known derivatives of diazoalkane and azine as the metastable intermediate or crosslinking moiety. The nanosecond lifetime of carbene species prevents direct

detection, but indirect evidence of N/O insertion peaks were found in the ^{19}F NMR spectra and the reduction of primary amine in FTIR spectra supports a singlet carbene intermediate similar in nature to thermal activation of diazirine[27, 36]. Other crosslinking mechanisms such as (i) amine oxidation at the anode, (ii) resonance of diazirine to negative hyperconjugation transition states, or (iii) Schiff-base formation by primary amines/ketones cannot be excluded[24, 26, 37-38].

The chosen frequency range of 0.008-12.5 Hz overlaps transcranial stimulation (1-64 Hz) that can adversely modulate brain neural activity. Transient adverse effects such as illusory visual percepts, dizziness, skin sensation, and pressure perception during stimulation peak at frequencies of 2, 4, and 16 Hz[39]. The optimized frequency for electrocuring is 0.050 Hz, which is still a safe frequency zone.

The proposed Voltaglue patch also presents an advancement over the previously reported electrode geometries for electrocuring. For instance, three electrode circuits for Voltaglue activation have the advantage of maintaining a constant voltage with a simple potentiostat, but the circuits have inherently limited working electrodes (cathode) less than 5 mm diameter[4], whereas the semiconducting surfaces in the Voltaglue patch demonstrate an increased activation area on the order of sq. cm. Interdigitated graphene electrodes allow rapid activation across a predetermined surface area, but no activation is observed over the anode[2]. Only 50-60 % area activation (no curing at anode) is observed under DC due to dissipating electric fields between the interdigitated electrodes. Changing polarity via AC cures the Voltaglue on all electrodes leading to >90 % surface activation (**Video S2**).

The observation that no electrocuring is observed at high frequencies allows interfacing with previous electroceutical wound treatments. For example, Aoki et al. have recently demonstrated that high-voltage AC stimulation (14 kV, 80 Hz) can induce transcriptional responses in keratinocytes. The small profile of the Voltaglue patch is an additional benefit compared to the oversized voltage incubator[40]. Other instances where a small profile AC stimulation may prove

useful include AC-induced calcium influx (1-2 V/mm, 1-10 Hz) and AC-enhanced osteogeneration (1.5 V/cm, 1 Hz)[41-42]. These oversized devices employ stiff metal/glass materials to interface with in-vivo environments. The proposed Voltaglue patch provides a platform where the electrodes can be shaped to the application. However, the Voltaglue patch requires a more robust semiconductive patch versus the current conductive paper. Replacement of the Teledeltos paper can be done with a number of flexible semiconductor substrates, such as graphene/polyaniline, polypyrrole, PEDOT: PSS, or reduced graphene oxide (rGO)[43-47]. Preliminary testing of the latter two materials displays positive results, but further optimization of resistance and geometry is required as seen in **Figure S5**. Electrochemical activation of Voltaglue is possible with more robust biocompatible substrates and this will be part of our future work. Microelectronic fabrication (e.g flip-chips), construction (e.g. window sealants), and medicine (e.g. tissue adhesives) are but a few industries that could benefit from electrocuring designs[5-9]. In addition, applications of Voltaglue could also be explored in the fields where PAMAM has been exploited such as— stimuli-responsive biomaterials, electrochemical sensors, conductive polymers, and controlled chemical release— all applications that can benefit from voltage-activated adhesion[10-17].

A few limitations of the scope and Voltaglue design should be noted. Amine/carbene insertions have been reported to produce toxic hydrofluoric acid[37]. However, current ^{19}F NMR and FTIR investigations do not reveal any peaks or other evidence of fluoride. Carbene fouling by water due to ^{-}OH insertion may explain the weaker mechanical properties of the electrocured matrix compared to photocured matrices that partially crosslink by diazoalkane[20, 37]. NMR results illustrate that the majority of diazirines are unreacted after electrocuring, which the current mechanism does not account for. The AC-frequency investigation may be dependent on a number of factors including the ionic profile/concentration, temperature, Voltaglue/diazirine concentration, and current magnitude. Further optimization on AC frequency parameters is

needed by substituting counter-cations and temperature. Future investigations of the electrocuring mechanism and parameters such as studying the effect of different frequency levels using NMR and FTIR aim to resolve these limitations and are part of our future work.

CONCLUSION

Voltaglue is electrocured using square wave alternating current (AC) electric fields, which gives considerable improvements over DC methods. Two-sided progression, lower peak voltages, and higher adhesion strengths result from optimized AC frequencies. Tunable mechanical properties (0.5-15 kPa), and lap shear adhesion (25-82 kPa) is significantly higher than DC electric field stimulation. The electrochemical reduction of diazirine (electrochemical crosslinker in Voltaglue) is seen to be frequency dependent, where low current electrocuring is optimized under 500 mHz, avoiding interference with neural activity frequencies.

ASSOCIATED CONTENT

Supporting Information

The Supporting Information is available free of charge via the Internet at http://pubs.acs.org.

Video S1 and Video S2 (mov)

Model and geometry of the Voltaglue Patch, summary of electrocuring under high magnitude constant DC stimulation, electrocuring progression over reduced graphene oxide (rGO) and PEDOT:PSS coated substrates under DC/ AC stimulation, and comparison of lap shear adhesion strength of voltaglue with commercial tissue sealants (PDF)

FUNDING SOURCES

This work is financially supported by the Ministry of Education (Singapore) Tier 2 Grant: Reversible, electrocuring adhesives (MOE2014-T2-2-100), NTU-Northwestern Institute for

Nanomedicine Grant: 3D-Printing of Electro-Curing Nanocomposite Living Electrodes for Cardiac Tissue Regeneration, Agency for Science, Technology and Research (A*Star) IRG17283008 'Microprocessor based methods of composite curing'

ACKNOWLEDGMENTS

The authors acknowledge the financial support from the Ministry of Education (Singapore) Tier 2 Grant: Reversible, electrocuring adhesives (MOE2014-T2-2-100), NTU-Northwestern Institute for Nanomedicine Grant: 3D-Printing of Electro-Curing Nanocomposite Living Electrodes for Cardiac Tissue Regeneration, Singapore Agency for Science, Technology and Research (A*STAR) AME IRG grant (IRG17283008). The authors would like to thank NTU-Interdisciplinary Graduate School scholarship program, and School of Materials Science and Engineering for all the research facilities provided. JVH acknowledges support for the solid state NMR instrumentation at Warwick used in this research which was funded by EPSRC and the University of Warwick, with additional partial funding being provided through the Birmingham Science City AM1 and AM2 projects which were supported by Advantage West Midlands (AWM) and the European Regional Development Fund (ERDF).

REFERENCES

1. Singh, M.; Webster, R. D.; J. Steele, T. W., Voltaglue Electroceutical Adhesive Patches for Localized Voltage Stimulation. *ACS Applied Bio Materials* **2019**, 2 (6), 2633-2642.

2. Singh, M.; Nanda, H. S.; O'Rorke, R. D.; Jakus, A. E.; Shah, A. H.; Shah, R. N.; Webster, R. D.; Steele, T. W. J., Voltaglue Bioadhesives Energized with Interdigitated 3D-Graphene Electrodes. *Adv Healthc Mater* **2018,** *7* (21), e1800538.

3. Gan, L.; Tan, N. C. S.; Shah, A. H.; Webster, R. D.; Gan, S. L.; Steele, T. W. J., Voltage-Activated Adhesion through Donor–Acceptor Dendrimers. *Macromolecules* **2018,** *51* (17), 6661-6672.

4. Ping, J.; Gao, F.; Chen, J. L.; Webster, R. D.; Steele, T. W., Adhesive curing through low-voltage activation. *Nat Commun* **2015,** *6*, 8050.

5. Yeon, J.; Song, Y.; Kim, K. K.; Kang, J., Effects of Epoxy Adhesive Layer Thickness on Bond Strength of Joints in Concrete Structures. *Materials (Basel)* **2019,** *12* (15).

6. Xia, S.; Song, S.; Jia, F.; Gao, G., A flexible, adhesive and self-healable hydrogel-based wearable strain sensor for human motion and physiological signal monitoring. *J Mater Chem B* **2019,** *7* (30), 4638-4648.

7. Persson, B. N. J.; Guo, J., Electroadhesion for soft adhesive pads and robotics: theory and numerical results. *Soft Matter* **2019**, 15 (40), 8032-8039.

8. Koivusalo, L.; Kauppila, M.; Samanta, S.; Parihar, V. S.; Ilmarinen, T.; Miettinen, S.; Oommen, O. P.; Skottman, H., Tissue adhesive hyaluronic acid hydrogels for sutureless stem cell delivery and regeneration of corneal epithelium and stroma. *Biomaterials* **2019,** *225*, 119516.

9. Blacklow, S. O.; Li, J.; Freedman, B. R.; Zeidi, M.; Chen, C.; Mooney, D. J., Bioinspired mechanically active adhesive dressings to accelerate wound closure. *Sci Adv* **2019,** *5* (7), eaaw3963.

10. Zhu, J.; Ye, Z.; Fan, X.; Wang, H.; Wang, Z.; Chen, B., A highly sensitive biosensor based on Au NPs/rGO-PAMAM-Fc nanomaterials for detection of cholesterol. *Int J Nanomedicine* **2019,** *14*, 835-849.

11. Smith, R. J.; Gorman, C. B.; Menegatti, S., DendriPeps: Expanding Dendrimer Functionality by Hybridizing Poly(amidoamine) (PAMAM) Scaffolds with Peptide Segments. *Macromol Rapid Commun* **2019**, e1900325.

12. Rodriguez-Fonseca, R. A.; Bello, M.; de Los Munoz-Fernandez, M. A.; Luis Jimenez, J.; Rojas-Hernandez, S.; Fragoso-Vazquez, M. J.; Gutierrez-Sanchez, M.; Rodrigues, J.; Cayetano-Castro, N.; Borja-Urby, R.; Rodriguez-Cortes, O.; Garcia-Machorro, J.; Correa-Basurto, J., In silico search, chemical characterization and immunogenic evaluation of amino-

terminated G4-PAMAM-HIV peptide complexes using three-dimensional models of the HIV-1 gp120 protein. *Colloids Surf B Biointerfaces* **2019,** *177*, 77-93.

13. Czarnomysy, R.; Bielawska, A.; Bielawski, K., Effect of 2nd and 3rd generation PAMAM dendrimers on proliferation, differentiation, and pro-inflammatory cytokines in human keratinocytes and fibroblasts. *Int J Nanomedicine* **2019,** *14*, 7123-7139.

14. Li, J.; Liang, H.; Liu, J.; Wang, Z., Poly (amidoamine) (PAMAM) dendrimer mediated delivery of drug and pDNA/siRNA for cancer therapy. *Int J Pharm* **2018,** *546* (1-2), 215-225.

15. Araujo, R. V.; Santos, S. D. S.; Igne Ferreira, E.; Giarolla, J., New Advances in General Biomedical Applications of PAMAM Dendrimers. *Molecules* **2018,** *23* (11).

16. Chandra, S.; Mayer, M.; Baeumner, A. J., PAMAM dendrimers: A multifunctional nanomaterial for ECL biosensors. *Talanta* **2017,** *168*, 126-129.

17. Zarghami, Z.; Akbari, A.; Latifi, A. M.; Amani, M. A., Design of a new integrated chitosan-PAMAM dendrimer biosorbent for heavy metals removing and study of its adsorption kinetics and thermodynamics. *Bioresour Technol* **2016,** *205*, 230-8.

18. Nanda, H.; Singh, M.; Steele, T. W. J., Thrombogenic Responses from Electrocured Tissue Adhesives. *ECS transactions* **2017,** *77* (11), 547-555.

19. Gan, L.; Tan, N. C. S.; Gupta, A.; Singh, M.; Pokholenko, O.; Ghosh, A.; Zhang, Z.; Li, S.; Steele, T. W. J., Self curing and voltage activated catechol adhesives. *Chemical Communications* **2019,** *55* (68), 10076-10079.

20. Feng, G.; Djordjevic, I.; Mogal, V.; O'Rorke, R.; Pokholenko, O.; Steele, T. W., Elastic Light Tunable Tissue Adhesive Dendrimers. *Macromol Biosci* **2016,** *16* (7), 1072-82.

21. Michael T.H. Liu, K. R., Mechanism for the formation of azine in the decomposition of diazo-alkanes and diazirines. *Tetrahedron Letters* **1977,** *36*, 3139 - 3142.

22. Grayston, M. W.; Lemal, D. M., Perfluorohexamethylbicyclopropenyl. *Journal of the American Chemical Society* **1976,** *98* (5), 1278-1280.

23. Korneev, S. M., Valence Isomerization between Diazo Compounds and Diazirines. *European Journal of Organic Chemistry* **2011,** *2011* (31), 6153-6175.

24. Moss, R. A., Diazirines: Carbene Precursors Par Excellence. *ACCOUNTS OF CHEMICAL RESEARCH* **2006** *39* (4), 267-272.

25. Elson, C. M.; Liu, M. T. H., Electrochemical behaviour of diazirines. *Journal of the Chemical Society, Chemical Communications* **1982**, (7), 415-416.

26. Fischer, K. H.; Hemberger, P.; Fischer, I.; Rijs, A. M., Infrared spectra of reactive species generated by flash pyrolysis in a free jet. *Chemphyschem* **2010,** *11* (15), 3228-30.

27. Blencowe, A.; Fagour, W.; Blencowe, C.; Cosstick, K.; Hayes, W., Synthesis of hyperbranched poly(aryl amine)s via a carbene insertion approach. *Org Biomol Chem* **2008,** *6* (13), 2327-33.

28. van Dommelen, J. A. W.; Hrapko, M.; Peters, G. W. M., Mechanical Properties of Brain Tissue: Characterisation and Constitutive Modelling. In *Mechanosensitivity of the Nervous System: Forewords by Nektarios Tavernarakis and Pontus Persson*, Kamkim, A.; Kiseleva, I., Eds. Springer Netherlands: Dordrecht, 2009; pp 249-279.

29. Ozawa, H.; Matsumoto, T.; Ohashi, T.; Sato, M.; Kokubun, S., Mechanical properties and function of the spinal pia mater. *Journal of neurosurgery. Spine* **2004,** *1* (1), 122-7.

30. Saraf, H.; Ramesh, K. T.; Lennon, A. M.; Merkle, A. C.; Roberts, J. C., Mechanical properties of soft human tissues under dynamic loading. *Journal of Biomechanics 40* (9), 1960-1967.

31. Kang, N.; Song, S. H.; Kyung, H.; Oh, S. H., Medpor Implant Fixation Using Fibrin Glue in the Treatment of Medial Orbital Wall Fracture. *The Journal of craniofacial surgery* **2015,** *26* (4), 1361-4.

32. Yoshida, H.; Hirozane, K.; Kamiya, A., Adhesive strength of autologous fibrin glue. *Biological & pharmaceutical bulletin* **2000,** *23* (3), 313-7.

554 33. Shannon, R. D., Revised effective ionic radii and systematic studies of interatomic
555 distances in halides and chalcogenides. *Acta Crystallographica Section A* **1976,** *32* (5), 751-
556 767.
557 34. Mähler, J.; Persson, I., A Study of the Hydration of the Alkali Metal Ions in Aqueous
558 Solution. *Inorganic Chemistry* **2012,** *51* (1), 425-438.
559 35. Wang, J.; Zhang, L.; Xue, J.; Hu, G., Ion diffusion coefficient measurements in
560 nanochannels at various concentrations. *Biomicrofluidics* **2014,** *8* (2), 024118.
561 36. Anton Blencowe, N. C., Kevin Cosstick,William Fagour,Peter Heath, Wayne Hayes,
562 Synthesis of Hyperbranched Poly(aryl ether)s via Carbene Insertion Processes.
563 *Macromolecules* **2007,** (40), 939-949.
564 37. Fleming, S. A., Chemical Reagents in Photoaffinity Labeling. *tetrahedron Lett* **1995,**
565 (385).
566 38. Fry, A. J., Organic Electrochemistry, Fourth Edition, Revised and Expanded Edited by
567 Henning Lund (Aarhus University) and Ole Hammerich (University of Copenhagen). Marcel
568 Dekker: New York and Basel. 2001. x + 1394 pp. $275.00. ISBN 0-8247-0430-4. *Journal of the*
569 *American Chemical Society* **2001,** *123* (36), 8880-8880.
570 39. Matsumoto, H.; Ugawa, Y., Adverse events of tDCS and tACS: A review. *Clin*
571 *Neurophysiol Pract* **2017,** *2*, 19-25.
572 40. Aoki, M.; Matsumoto, N. M.; Okubo, Y.; Ogawa, R., Cytochrome P450 genes play
573 central roles in transcriptional response by keratinocytes to a high-voltage alternating current
574 electric field. *Bioelectrochemistry* **2019,** *126*, 163-171.
575 41. Cho, M. R.; Thatte, H. S.; Lee, R. C.; Golan, D. E., Reorganization of microfilament
576 structure induced by ac electric fields. *FASEB journal : official publication of the Federation of*
577 *American Societies for Experimental Biology* **1996,** *10* (13), 1552-8.

42. Huang, Y.; Deng, H.; Fan, Y.; Zheng, L.; Che, J.; Li, X.; Aifantis, K. E., Conductive nanostructured Si biomaterials enhance osteogeneration through electrical stimulation. *Materials Science and Engineering: C* **2019**, 103, 109748.

43. Das, S. R.; Uz, M.; Ding, S.; Lentner, M. T.; Hondred, J. A.; Cargill, A. A.; Sakaguchi, D. S.; Mallapragada, S.; Claussen, J. C., Electrical Differentiation of Mesenchymal Stem Cells into Schwann-Cell-Like Phenotypes Using Inkjet-Printed Graphene Circuits. *Adv Healthc Mater* **2017,** *6* (7).

44. Jakus, A. E.; Secor, E. B.; Rutz, A. L.; Jordan, S. W.; Hersam, M. C.; Shah, R. N., Three-Dimensional Printing of High-Content Graphene Scaffolds for Electronic and Biomedical Applications. *ACS Nano* **2015,** *9* (4), 4636-4648.

45. Cuttaz, E.; Goding, J.; Vallejo-Giraldo, C.; Aregueta-Robles, U.; Lovell, N.; Ghezzi, D.; Green, R. A., Conductive elastomer composites for fully polymeric, flexible bioelectronics. *Biomaterials Science* **2019,** *7* (4), 1372-1385.

46. Liu, Y.; Zhang, B.; Xu, Q.; Hou, Y.; Seyedin, S.; Qin, S.; Wallace, G. G.; Beirne, S.; Razal, J. M.; Chen, J., Development of Graphene Oxide/Polyaniline Inks for High Performance Flexible Microsupercapacitors via Extrusion Printing. *Advanced Functional Materials* **2018,** *28* (21), 1706592.

47. George, P. M.; Lyckman, A. W.; LaVan, D. A.; Hegde, A.; Leung, Y.; Avasare, R.; Testa, C.; Alexander, P. M.; Langer, R.; Sur, M., Fabrication and biocompatibility of polypyrrole implants suitable for neural prosthetics. *Biomaterials* **2005,** *26* (17), 3511-3519.

602 **TOC**

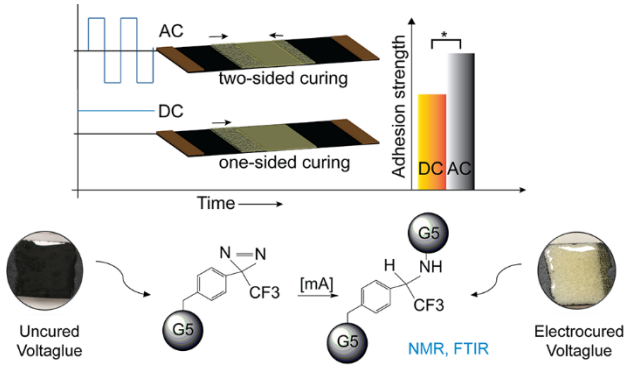

603

604

605 **COVER PAGE**

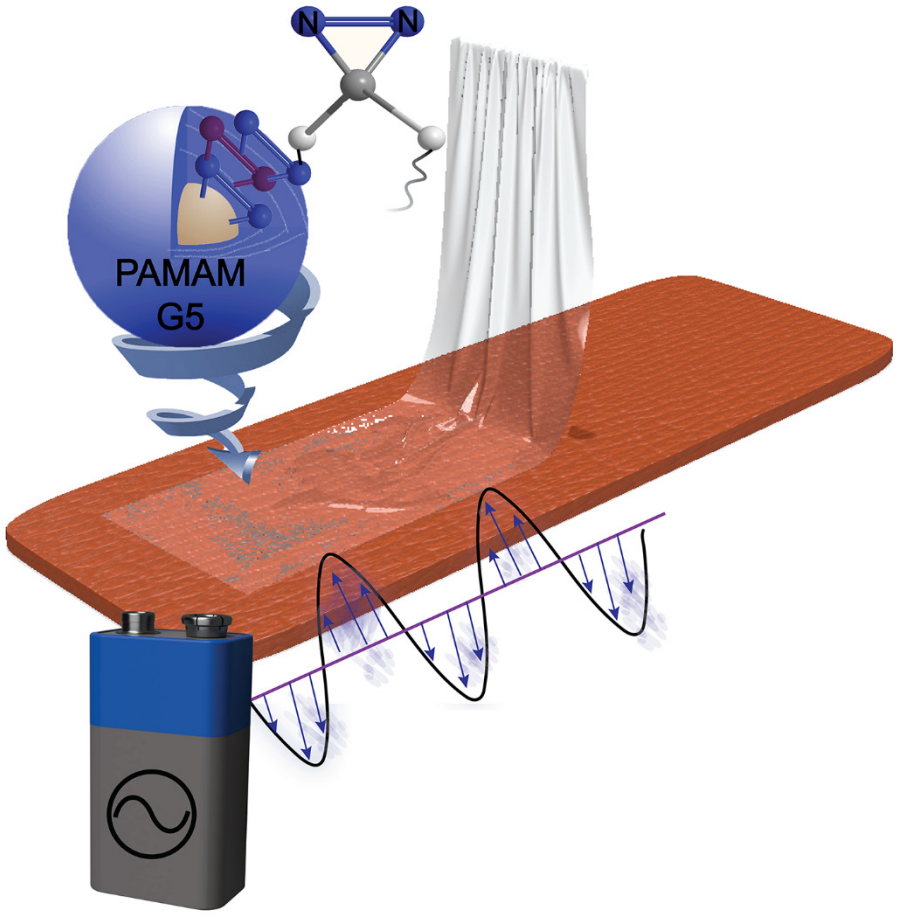

606

Supplementary Information

Synergistic Voltaglue adhesive mechanisms with alternating electric fields

*Manisha Singh[1,2], Cheong See Yin[2], Samuel J. Page[3], Yuqing Liu[4,5], Gautama Wicaksono[2], Rajashekhar Pujar[6], Shyam Kumar Choudhary[7], Giridhar U. Kulkarni[6], Jun Chen[4], John V. Hanna[2,3], Richard D. Webster[8], Terry W. J. Steele[1,2]**

[1]NTU-Northwestern Institute for Nanomedicine (NNIN), Interdisciplinary Graduate School (IGS), Nanyang Technological University (NTU), 50 Nanyang Drive, Singapore 637553

[2]School of Materials Science and Engineering (MSE), Nanyang Technological University (NTU), Singapore 639798

[3]Department of Physics, University of Warwick, Coventry CV4 7AL, United Kingdom

[4]ARC Centre of Excellence for Electromaterials Science, Intelligent Polymer Research Institute (IPRI), Australian Institute of Innovative Materials (AIIM), University of Wollongong, Wollongong, NSW 2522, Australia

[5]State Key Laboratory of Electronic Thin Film and Integrated Devices, University of Electronic Science and Technology of China, Chengdu, 610054, China.

[6]Centre for Nano and Soft Matter Sciences, Jalahalli, Bengaluru 560013, India

[7]Tata steel LTD, Jamshedpur 831001, India

[8]Division of Chemistry and Biological Chemistry, School of Physical and Mathematical Sciences, Nanyang Technological University, Singapore 637371

*Correspondence to Terry W. J. Steele (e-mail: wjsteele@ntu.edu.sg)

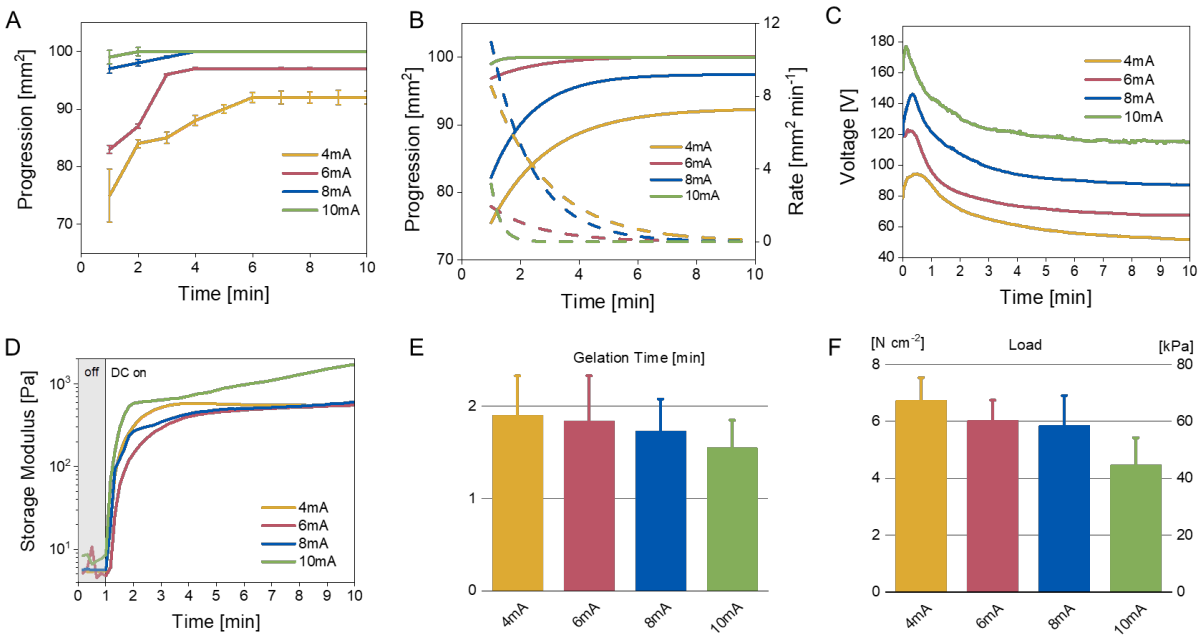

Figure S1: Summary of electrocuring under high magnitude constant DC stimulation (4- 10 mA) —electric fields of 90-180 V/30 mm. A) Surface area progression of electrocuring at direct current. B) Fitted curves and derivatives of surface area progression of electrocuring at different constant direct current (4- 10mA). C) Representative voltage recordings against the time during Voltaglue electrocuring. D) Storage modulus (G') before and after DC stimulation (4- 10 mA). E) Gelation time (defined as the time to reach G"/G' = 1) against constant current applied. F) Maximum adhesive shear strength at failure after 10 min of electrocuring. Data presented as mean ± SD, n = 3, p-values are calculated using one-way ANOVA with Tukey correction, *p < 0.05.

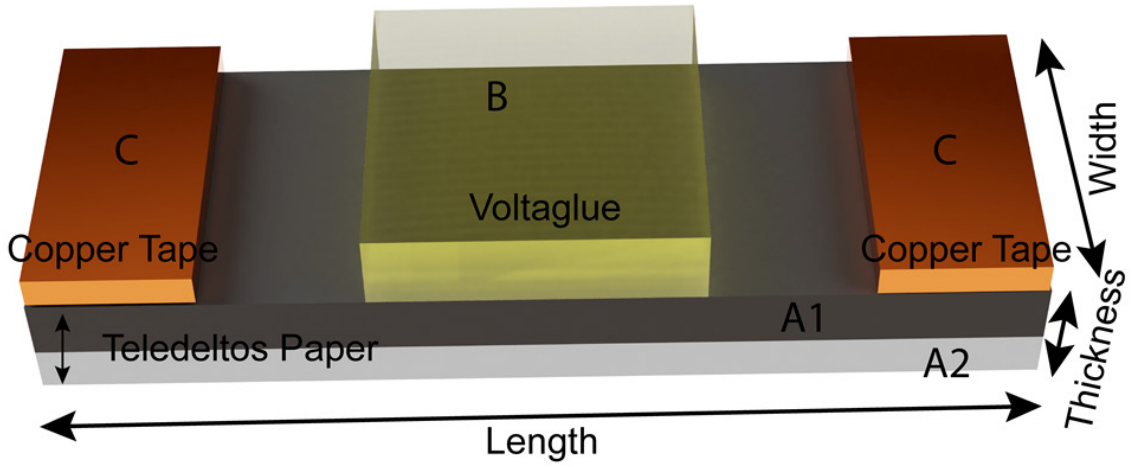

Figure S2: Model and geometry of the Voltaglue Patch.

Table S1: Geometry of the Voltaglue patch				
Label	Section Name	Thickness (mm)	Length (mm)	Width (mm)
A1	Conductive coating on Teledeltos Paper	0.1	40	10
A2	Cellulose backing of Teledeltos Paper	0.1	40	10
B	Voltaglue*	0.3	10	10
C	Copper tape	0.1	5	10
*Voltaglue is placed equidistant from anode and cathode copper adhesive tape terminals.				

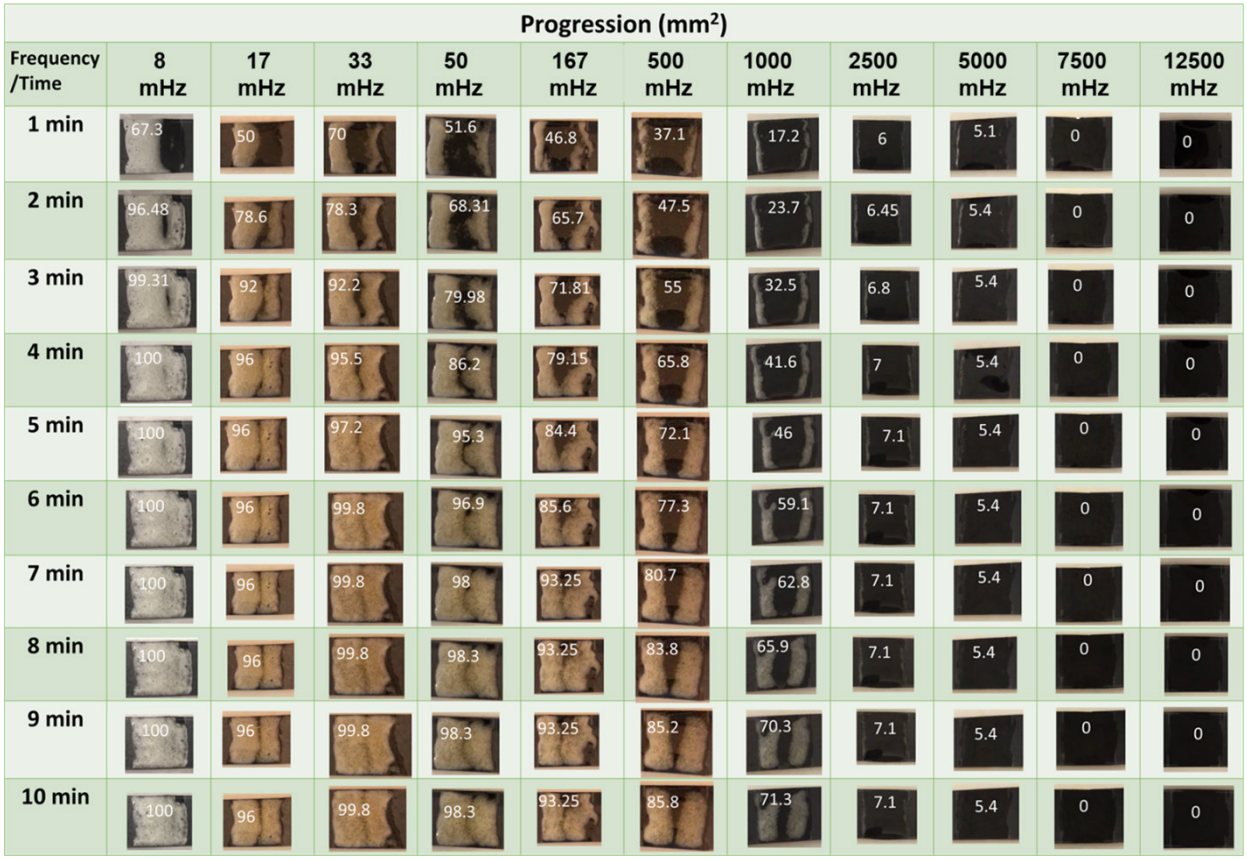

Figure S3: Digital images of two-sided electrocuring progression over a 10-min interval under an alternating current of 3 mA (8 mHz-12500 Hz).

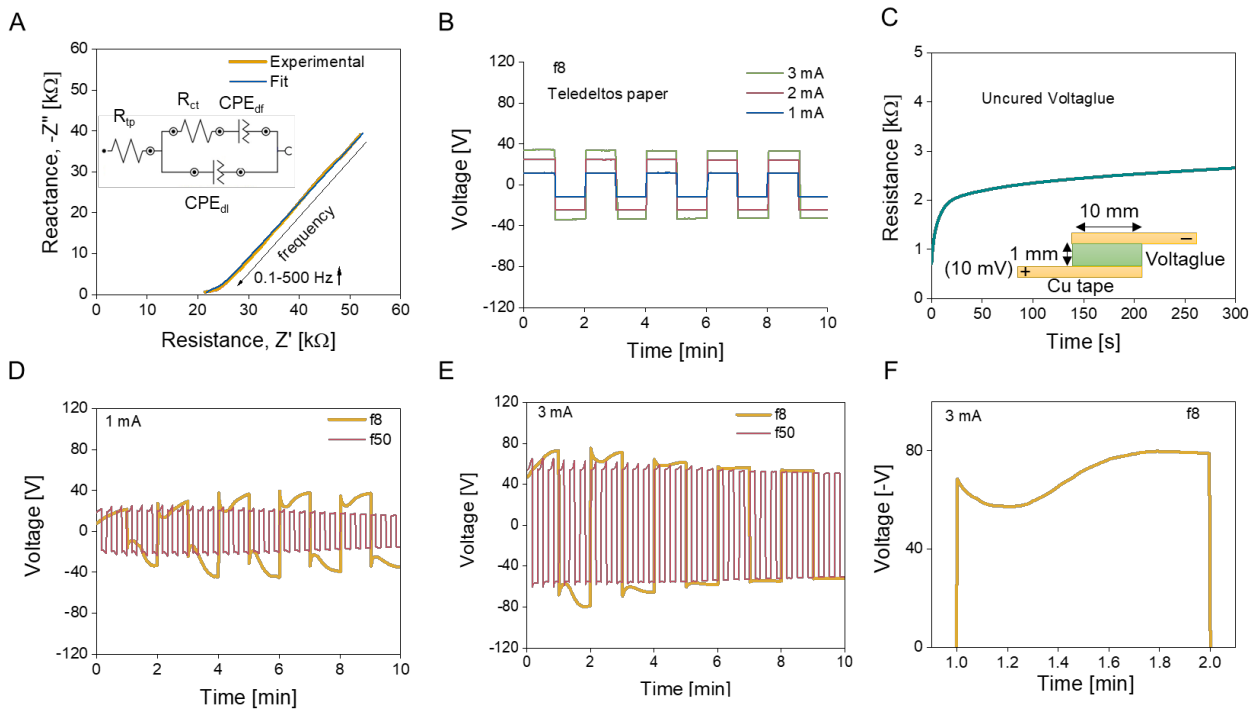

Figure S4: Overview of voltage vs time recordings. A) Complex plane impedance plot obtained for uncured Voltaglue at AC amplitude: 10 mV; frequency: 0.1- 500 Hz. Inset represents the equivalent electrical circuit model derived from the EIS data. B) Representative voltage vs. time recordings for Teledeltos paper electrodes. C) Representative resistance vs. time of uncured Voltaglue; measured using Keithley 2450 Sourcemeter at 10 mV. Inset represents the measurement setup configuration. D) Representative voltage recordings during electrocuring of Voltaglue for 1 mA, AC at frequencies of 8 and 50 mHz. E) Representative voltage recordings during electrocuring of Voltaglue for 3 mA, AC at frequencies of 8 and 50 mHz. F) Representative voltage recordings (magnified to half wave period) during electrocuring of Voltaglue for 3 mA, AC at frequency of 8 mHz.

Table S2: Summary of electrochemical components from EIS data fit		
Component	Name	Value
R_{tp}	Resistance of Teledeltos paper	21.7 kΩ
R_{ct}	Charge transfer resistance at the Voltaglue-Teledeltos paper interface	2.63 kΩ
CPE_{dl}	Constant phase element that models the double layer impedance at the interface	1.45 $\mu S \cdot s^n$ n= 0.867
CPE_{df}	Constant phase element that models the diffusion process of ions	25.9 $\mu S \cdot s^n$ n= 0.588

A spectrum for lower frequencies 500-0.1 Hz is plotted in Figure S4A. The experimental data are fitted using Nova 2.1 and the corresponding electrical circuit is also displayed in Figure S4A inset. The corresponding values and labels of all the electrochemical components are presented in Table S2. The resistance of Teledeltos paper (R_{tp}) estimated from this fitted plot is 21.7 kΩ, which is comparable to the experimental results obtained from the voltage vs. time transients (Figure S4B) under the application of square wave AC for Teledeltos paper alone. The charge transfer resistance (R_{ct}) at the interface is 2.63 kΩ which is very similar to the resistance of uncured Voltaglue as measured experimentally (Figure S4C). A region, very close to Warburg for lower frequencies is obtained where n is 0.588 for CPE_{df}. The Warburg diffusion element is

an equivalent electrical circuit component that models the diffusion process of small ions (i.e. K^+, Na^+, Cl^-, H^+, etc.) involved in the electrocuring.

Table S3. Rate constant (k) of the surface progression.		
Parameters	**Current (mA)**	**Rate constant (min^{-1})***
8 mHz (120 s/cycle)	1	0.63
	2	0.64
	3	1.20
17 mHz (60 s/cycle)	1	0.75
	2	1.69
	3	0.81
50 mHz (20 s/cycle)	1	0.63
	2	1.78
	3	0.63
167 mHz (6 s/cycle)	1	0.53
	2	0.57
	3	0.59
500 mHz (2 s/cycle)	1	0.14
	2	0.49
	3	0.38
DC	1	0.15
	2	0.52
	3	1.14

DC 4°C	2	0.37
DC 24°C	2	0.72
DC 50°C	2	0.76
DC K^+	2	0.39
DC Na^+	2	0.72
DC Li^+	2	0.75
*rate constant (k) is reported with an error of ± 10%.		

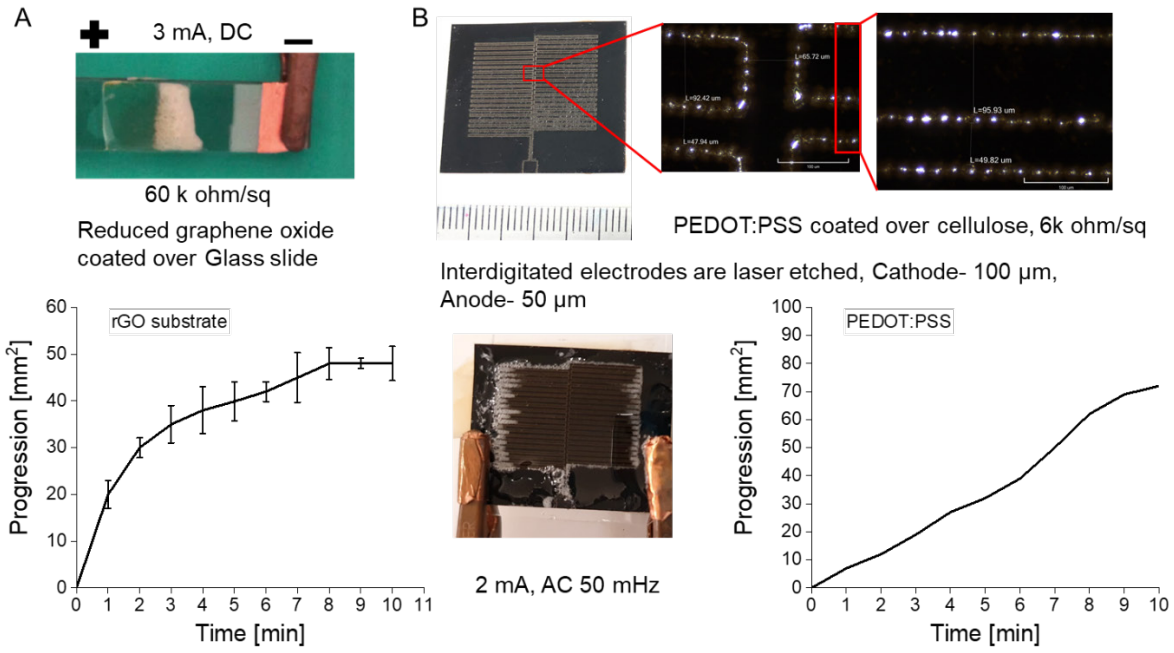

Figure S5: Summary of electrocuring progression over reduced graphene oxide (rGO) and PEDOT:PSS coated substrates under DC/ AC stimulation.

Amplitude sweep measurements are performed at a constant angular frequency of 1 Hz under various strains of 0.1 to 1000 %. The yield stress (τ_y) is plotted against frequency (8-50 mHz) in

Figure S6B. The τ_y of the electrocured Voltaglue increased with increasing frequency of 2 mA AC, and the slope of the plot is determined to be 0.4 (i.e. $\tau_y \propto f^{0.4}$) in the frequency range tested.

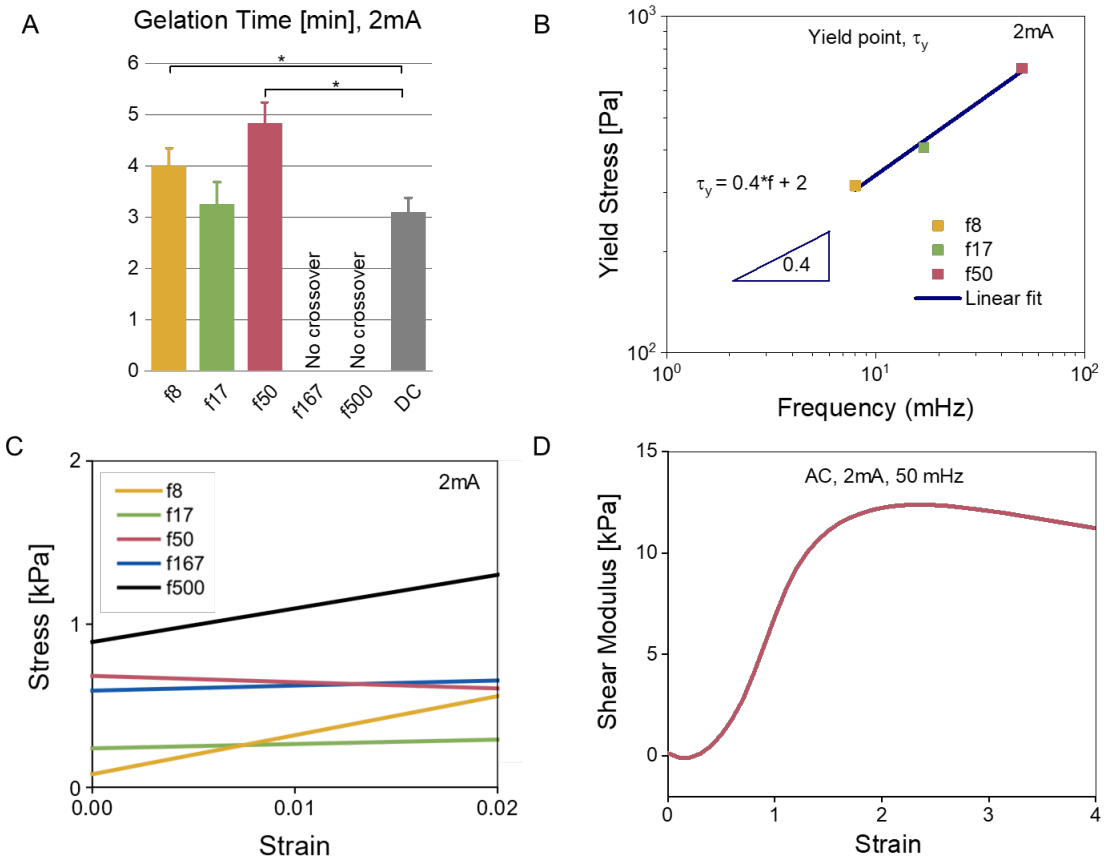

Figure S6: Mechanical properties and shear adhesion strength. A) Real-time electrorheology of Voltaglue patch. Gelation time (defined as the time to reach G"/G' = 1) against constant current applied. No crossover is observed for 167 and 500 mHz. B) Dynamic yield stress as a function of 2 mA, AC frequency for electrocured Voltaglue. C) Magnified stress vs. strain plot from Figure 4D to represent stress corresponding to strain < 2%. D) Shear modulus vs. strain, calculated from shear stress vs. shear strain plots (Figure 4D) for 2 mA, AC at 50 mHz. Data presented as mean ± SD, n = 3, p-values are calculated using one-way ANOVA with Tukey correction, *p < 0.05.

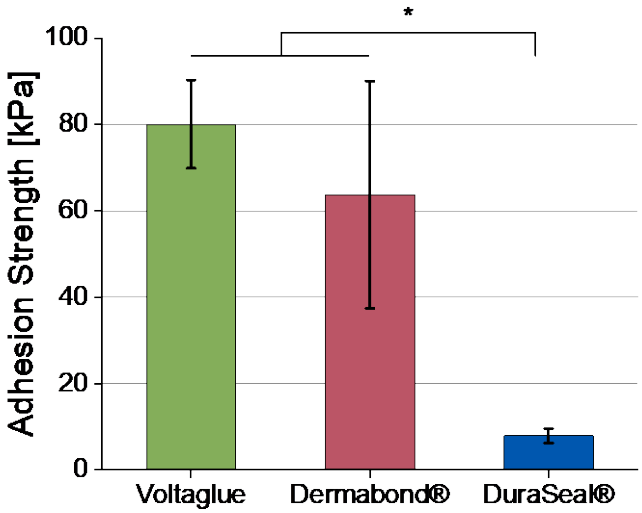

Figure S7: Lap shear adhesion strength of voltaglue (2 mA, AC, 50 mHz) and commercial tissue sealants — Dermabond® and DuraSeal® against hydrated collagen substrates. Data presented as mean ± SD, n = 3, p-values are calculated using one-way ANOVA with Tukey correction, *p < 0.05.

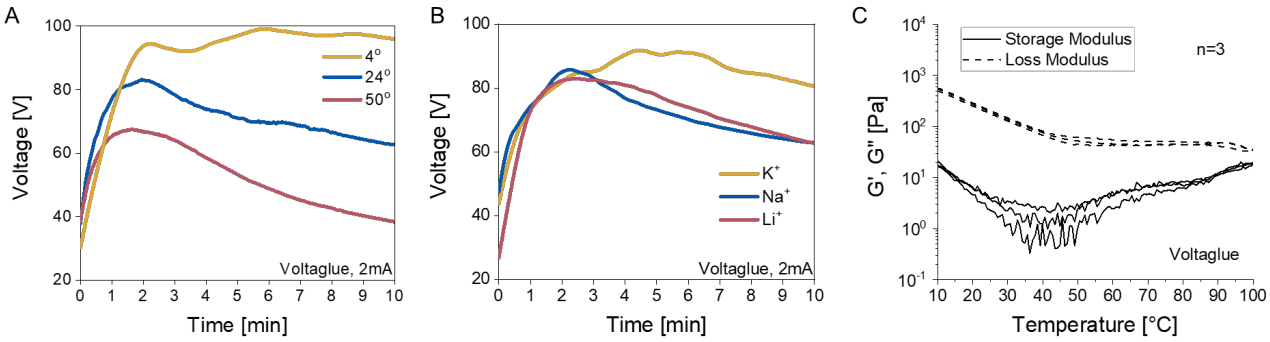

Figure S8: Summary of electrocuring for different temperature (4, 24, or 50 °C) and ionic (K^+, Na^+, or Li^+) conditions. A) Representative voltage recordings against the time during Voltaglue electrocuring at different temperatures (4, 24, or 50 °C). B) Representative voltage recordings against the time during Voltaglue electrocuring at different ionic (K^+, Na^+, or Li^+) conditions in

PBS. C) Temperature sweep (10- 100 °C) of Voltaglue at 1 % strain and 1 Hz frequency using rheometer.

The composition of PBS (1X)- NaCl

Salt	Concentration (mmol/L)	Concentration (g/L)
NaCl	137	8.0
KCl	2.7	0.2
Na_2HPO_4	10	1.44
KH_2PO_4	2	0.24

The composition of PBS (1X)- LiCl

Salt	Concentration (mmol/L)	Concentration (g/L)
LiCl	137	5.81
KCl	2.7	0.2
Na_2HPO_4	10	1.44
KH_2PO_4	2	0.24

The composition of PBS (1X)- KCl

Salt	Concentration (mmol/L)	Concentration (g/L)
KCl	137	10.21
KCl	2.7	0.2
K_2HPO_4	10	1.74
KH_2PO_4	2	0.24

Figure S9: The recipe of the saline solvents used to prepare counter-cation (K^+, Na^+, or Li^+) formulations.